Research Article

Algae 2026, 41(3): 347-360
https://doi.org/10.4490/algae.2026.41.9.9

Open Access

Physiological and photosynthetic characteristics associated with photoprotection in a Korean strain of the green microalga *Haematococcus*

Gueeda Kim[1], Seunghye Park[2,*] and EonSeon Jin[1,2,3,*]

[1]*Department of Environmental Science, Hanyang University, Seoul 04763, Korea*
[2]*Department of Life Science, Hanyang University, Seoul 04763, Korea*
[3]*Hanyang Institute of Bioscience and Biotechnology, Hanyang University, Seoul 04763, Korea*

Haematococcus lacustris, a freshwater microalga, is known for its environmental resilience and ability to produce the high-value ketocarotenoid astaxanthin. In this study, a novel *H. lacustris* strain, HYU5231, was isolated and examined for phylogenetic position, morphology, growth, and photoprotective responses. Phylogenetic analyses using 18S rRNA, internal transcribed spacer, and Rubisco large subunit sequences confirmed that HYU5231 belongs to the *H. lacustris* lineage. Compared with the reference strain *H. lacustris* UTEX 2505, HYU5231 exhibited a larger cell size, lower pigment content, and comparable biomass productivity. Under increasing irradiance, HYU5231 exhibited a consistent photosystem II maximum quantum efficiency (F_V/F_M > 0.5) and showed increased non-photochemical quenching (NPQ) and accumulation of astaxanthin and carotenoids. The peak in NPQ with rapid astaxanthin accumulation suggests complementary photoprotective roles during prolonged exposure to high-intensity light. To investigate the photoprotection mechanisms, photosynthetic electron transport inhibitors were used, and chlorophyll fluorescence was assessed using pulse-amplitude-modulated fluorometry. HYU5231 exhibited higher NPQ but lower electron transport rates than UTEX 2505. Unlike UTEX 2505, dithiothreitol (DTT) did not suppress NPQ in HYU5231 cells, indicating that NPQ in this strain is not predominantly dependent on a DTT-sensitive xanthophyll cycle pathway. In contrast, propyl gallate markedly suppressed NPQ in HYU5231 cells, suggesting a potential contribution of plastid terminal oxidase (PTOX)-associated electron flow to photoprotection. Furthermore, methyl viologen increased electron transport in HYU5231 cells, suggesting a limitation on the photosystem I electron acceptor side. Collectively, these results reveal a distinct photoprotective strategy in HYU5231 and suggest a potential role for PTOX-associated alternative electron transport in maintaining photosynthetic performance under intense light conditions.

Keywords: *Haematococcus lacustris*; non-photochemical quenching (NPQ); photoprotection; photosynthetic electron transport; plastid terminal oxidase (PTOX)

Abbreviations: DES, de-epoxidation state; DTT, dithiothreitol; ETR, electron transport rate; F_V/F_M, maximum quantum efficiency of photosystem II; HL, high light; HPLC, high-performance liquid chromatography; HS, Sueoka high salts medium (composition detailed in text); ITS, internal transcribed spacer; LL, low light; ML, medium light; MV, methyl viologen; NJ, neighbor-joining; NPQ, non-photochemical quenching; PAM, pulse-amplitude-modulated (fluorometry); PAR, photosynthetically active radiation; PCR, polymerase chain reaction; PG, propyl gallate; PQ, plastoquinone; PSI, photosystem I; PSII, photosystem II; PTOX, plastid terminal oxidase; ΔpH, proton gradient (delta pH); ROS, reactive oxygen species; TAP, tris-acetate-phosphate

This is an Open Access article distributed under the terms of the Creative Commons Attribution Non-Commercial License (http://creativecommons.org/licenses/by-nc/4.0/) which permits unrestricted non-commercial use, distribution, and reproduction in any medium, provided the original work is properly cited.

Received June 25, 2026, **Accepted** September 9, 2026

***Corresponding Author**

E-mail: esjin@hanyang.ac.kr (E. Jin), eins21@hanmail.net (S. Park)
Tel: +82-2-2220-2561, Fax: +82-2-2266-2561

INTRODUCTION

Microalgae are major primary producers that contribute substantially to global oxygen production and biogeochemical cycling (Metting 1996, Lacour et al. 2020). These organisms thrive in diverse environments and have developed resilience to a wide range of environmental stresses, including fluctuations in light, temperature, salinity, and nutrient limitation (Seckbach et al. 2007, Teoh et al. 2013). Their ecological success is largely attributed to their ability to modify photosynthetic activity and activate photoprotective mechanisms that minimize light-induced damage.

Among these mechanisms, non-photochemical quenching (NPQ) plays a central role by dissipating excess absorbed light energy as heat when photon absorption exceeds the photochemical use. NPQ protects the photosynthetic apparatus from photooxidative damage and can be quantified using chlorophyll fluorescence and pulse-amplitude-modulated (PAM) fluorometry. The regulation of NPQ involves several processes, including xanthophyll cycle activity, proton gradient (ΔpH)-dependent changes in light-harvesting complexes, and redox regulation linked to photosynthetic electron transport (Demmig-Adams 1990, Müller et al. 2001, Niyogi and Truong 2013).

In addition to NPQ, photosynthetic organisms utilize alternative electron transport pathways to prevent overreduction of the photosynthetic electron transport chain. A crucial element of these pathways is plastid terminal oxidase (PTOX), which transfers electrons from the plastoquinone (PQ) pool to molecular oxygen. PTOX serves as an alternative electron sink, aiding in the maintenance of redox balance and safeguarding the photosynthetic apparatus under environmental stress conditions (Carol and Kuntz 2001). These alternative pathways may be particularly relevant in stress-tolerant algae, in which balancing photosynthetic electron flow with a robust photoprotective capacity is essential.

Haematococcus lacustris is a freshwater green microalgal species known for its exceptional tolerance to environmental stress and capacity to accumulate astaxanthin, a potent antioxidant carotenoid, under environmental stress (Boussiba 2000). Owing to its capacity for astaxanthin accumulation, *Haematococcus* has been extensively investigated for the optimization of cultivation strategies aimed at enhancing biomass and astaxanthin production (Sun et al. 2015). In addition to the xanthophyll cycle, photoprotection in *H. lacustris* involves several regulatory elements, including PsbS- and light-harvesting complex stress-related-mediated NPQ pathways (Peers et al. 2009, Correa-Galvis et al. 2016). Comparative studies have shown that the relative contributions of these photoprotective mechanisms vary considerably among photosynthetic organisms and can be dynamically adjusted during stress acclimation (Niyogi and Truong 2013, Ruban 2016).

In this study, a newly isolated *Haematococcus* strain was identified and characterized based on its morphological and growth characteristics. To investigate the photophysiological characteristics, chlorophyll fluorescence responses of the strain were analyzed following treatment with inhibitors targeting various stages in the photosynthetic electron transport chain. By comparing the effects of these inhibitors on NPQ and electron transport activity, we aimed to identify the major photoprotective pathways in this strain. These results provide insights into the diversity of photoprotective strategies in natural *Haematococcus* isolates and may support future applications of stress-induced metabolism and astaxanthin production.

MATERIALS AND METHODS

Algal strain isolation and culture conditions

Environmental samples were collected in November 2023 from a shallow rock pool near the Hantan River basin (38°00′29.04″ N, 127°04′31.00″ E), Gyeonggi-do, Republic of Korea (Fig. 1). Single colonies were isolated by serial dilution on tris-acetate-phosphate (TAP) agar plates (1.5% agar) supplemented with 50 μM kanamycin to suppress bacterial contamination during the initial isolation step. Colonies exhibiting characteristic red pigmentation were purified multiple times and subsequently transferred to liquid TAP medium for further purification. A stable monoclonal culture was established and used for subsequent physiological and molecular analyses. The Sueoka high salts medium (Sueoka 1960) contained 9.35 mM NH_4Cl, 0.070 mM $CaCl_2 \cdot 2H_2O$, 0.080 mM $MgSO_4 \cdot 7H_2O$, 8.27 mM K_2HPO_4, 5.29 mM KH_2PO_4, 537 μM EDTA, 18 μM $FeSO_4 \cdot 7H_2O$, 921 μM H_3BO_3, 765 μM $ZnSO_4 \cdot 7H_2O$, 512 μM $MnCl_2 \cdot 4H_2O$, 12 μM $CuSO_4 \cdot 5H_2O$, 17.8 μM $(NH_4)_6Mo_7O_{24} \cdot 4H_2O$, 135 μM $CoCl_2 \cdot 6H_2O$. All media were autoclaved at 121°C and 15 psi for 20 min. Cultures were maintained at 20–25°C in a growth chamber under low-light (LL, 40 μmol photons m^{-2} s^{-1}).

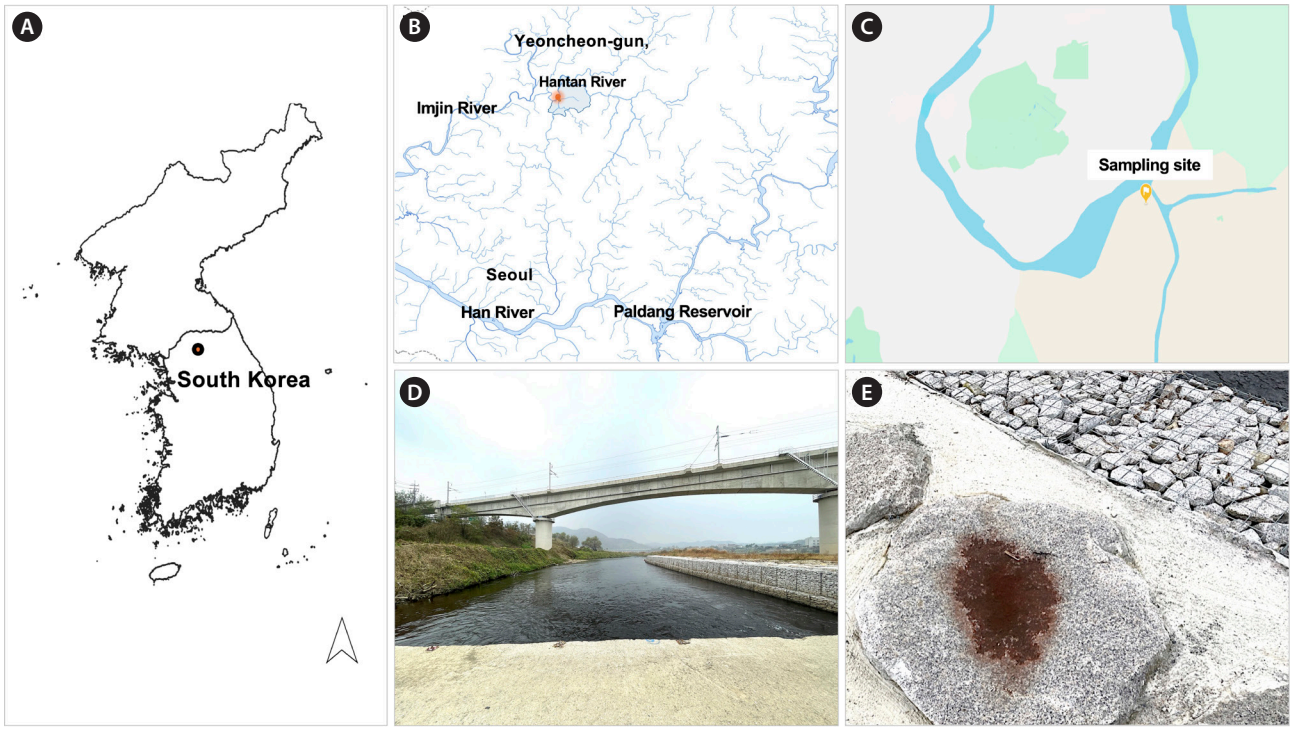


Fig. 1. Sampling location of *Haematococcus lacustris* strain HYU5231. (A) Overview of the sampling region within the Korean Peninsula. (B) Hydrological map of northern Gyeonggi Province showing the Hantan River, which lies north of Seoul. (C) The sampling site is situated along the outer section of an artificially modified channel, just upstream from where it joins the Hantan River. (D) Field photograph of the artificial channel located near the Hantan River. (E) A red-colored puddle on the rock surface, from which *H. lacustris* HYU5231 was isolated.

For light-intensity tests, cells were grown under medium light (ML, 150 µmol photons m^{-2} s^{-1}) or high light (HL, 500 µmol photons m^{-2} s^{-1}).

Phylogenetic analysis

Genomic DNA was extracted using a modified cetyltrimethylammonium bromide protocol (Fawley and Fawley 2004) to enhance yield and reduce polysaccharide contaminants. Approximately 300 ng of purified genomic DNA was used as a template for polymerase chain reaction (PCR) amplification of three molecular markers: the 18S rRNA gene (18S rRNA), the internal transcribed spacer (ITS) region, and the rbcL gene, using the primer sets listed in Table 1. PCR was performed using 20 µL (total volume) KOD One DNA polymerase (Toyobo, Osaka, Japan) according to the manufacturer's instructions. The thermal cycling conditions involved an initial denaturation at 95°C for 3 min, followed by 34 cycles of 95°C for 10 s, annealing at 52°C for 5 s, and extension at 68°C for 30 s, concluding with a final extension at 68°C for 5 min. Cycling parameters were adjusted as necessary in accordance with the manufacturer's guidelines. PCR products were purified and sequenced using the standard Sanger method. Sequence identities were assessed against the National Center for Biotechnology Information (NCBI) database using BLAST. Multiple sequence alignments of the 18S rRNA, ITS, and rbcL datasets were generated using multiple sequence alignment program using fast Fourier transform (MAFFT, online server: FFT-NS-2 algorithm) with the default parameters (Lee et al. 2025). Phylogenetic analyses were conducted using MEGA 11 software. The 18S rRNA phylogeny was inferred using the neighbor-joining (NJ) method based on the Maximum Composite Likelihood model, applying gamma-distributed rate heterogeneity ($\alpha = 1.0$), partial deletion (95% site coverage cutoff), and 500 bootstrap replicates. The ITS phylogeny was inferred using the NJ method with the Kimura 2-parameter model, pairwise deletion, and 1,000 bootstrap replicates. The rbcL phylogeny was reconstructed using the maximum likelihood method under the general time-reversible model, with gamma-distributed rate variation among sites (Γ; 10 categories), complete deletion of sites containing gaps or missing data, and 1,000 bootstrap replicates.

Details of the 18S, ITS, and rbcL sequences used for the phylogenetic analyses are provided in Supplementary Table S1.

Evaluation of cell growth and morphological characteristics

Cell growth was evaluated by measuring cell density and biomass. Cell density was measured by counting the cells using a hemocytometer under a light microscope (CH30-213E; Olympus, Tokyo, Japan), with three replicate measurements for each sample. Biomass was determined after centrifuging 10 mL of culture at 3,000 ×g for 5 min at 25°C, removing the supernatant, and drying the cell pellet at 60°C for 24 h to a constant weight. For morphological observations, 10 µL of well-mixed culture was placed on a glass slide and examined using a fluorescence microscope (Eclipse Ni; Nikon, Tokyo, Japan). Cell size was estimated based on the projected cell area measured from images of 100 randomly selected cells using the Nikon Imaging Software—Elements Basic Research (NIS-Elements BR) software. The specific growth rate (µ) was calculated during the exponential growth phase using the equation $\mu = (\ln X_2 - \ln X_1)/\Delta t$, where X_1 and X_2 represent the initial and final cell density, respectively. Doubling time was calculated as ln(2)/µ (Imamoglu et al. 2007).

Pigment analysis and calculation of the de-epoxidation state

Pigments were extracted from the algal cells with 90% (v/v) acetone using a cordless motorized pestle (KIMBLE, Vineland, NJ, USA) for 3 min, following Yuan and Chen (2000). The extracts were centrifuged at 13,000 rpm for 5 min, and the supernatant was filtered through a 0.2 µm nylon membrane prior to high-performance liquid chromatography (HPLC) analysis. Pigment separation was carried out using a Shimadzu Prominence HPLC system (LC-20AD; Shimadzu, Kyoto, Japan) fitted with a Waters Spherisorb S5 ODS-1 column (4.6 × 250 mm; Waters, Milford, MA, USA). A solvent gradient was used to separate the chlorophyll derivatives and carotenoids as described by Park et al. (2010), and absorbances were detected at 440 and 662 nm. The pigments were identified based on their retention times and quantified using external calibration curves. The xanthophyll cycle pigments, violaxanthin (V), antheraxanthin (A), and zeaxanthin (Z), were quantified from the chromatograms. The de-epoxidation state (DES) was calculated as DES = (A + Z)/(V + A + Z) (Demmig-Adams 1990).

PAM fluorometric analysis of photosynthetic performance

The chlorophyll fluorescence parameters, including the maximum quantum efficiency of photosystem II (PSII; F_V/F_M), NPQ, and electron transport rate (ETR), were measured using an Imaging-PAM fluorometer (Walz GmbH, Effeltrich, Germany).

For each assay, 200 µL of mid-log phase algal culture was placed into a black 96-well microplate, and the samples were dark-adapted for 15 min prior to measurement. In experiments involving inhibitors, dithiothreitol (DTT), n-propyl gallate (PG), and methyl viologen (MV) were used as inhibitors. The concentrations tested were 0.3–1.0 mM for DTT, 0.5–3.0 mM for PG, and 0.3–2.4 mM for MV, with concentrations of 0.3 mM DTT, 0.5 mM PG, and 1.2 mM MV chosen for further study. The inhibitors were added to the cell suspension under dark conditions and incubated for 15 min. Fluorescence signals were recorded using standard pulse amplitude modulation procedures (Bilger and

Table 1. The primers used in this study

Molecular marker	Primer	Nucleotide sequence 5' to 3'	Reference
SSU	EukA	GTCAGAGGTGAAATTCTTGGATTTA	Kim et al. (2022)
	EukB	AGGGCAGGGACGTAATCAACG	
ITS	ITS1	TCCGTAGGTGAACCTGCGG	Azúa-Bustos et al. (2010)
	ITS4	TCCTCCGCTTATTGATATGC	
rbcL	Dun FW1	GCTTTCCGTATGACACCTCAA	Won et al. (2023)
	Dun Rv2	AGTTTTAGCTAAAACACGGAA	
	F3	GCT TAC CGT GTA GAT CCA GTT CC	
	R3	CCT TCT AAT TTA CCA ACA ACT G	

Björkman 1990). In DTT-treated samples, chlorophyll fluorescence was measured immediately after inhibitor addition and again after 30 min of high-light exposure. Measurements were performed in triplicate.

NPQ was calculated as (Fm - Fm')/Fm', whereas ETR was calculated as 0.2× Φ PSII × photosynthetically active radiation (PAR) × 0.84 (μmol electrons m^{-2} s^{-1}) (Maxwell and Johnson 2000). The relationship between ETR and PAR was fitted using the Eilers and Peeters model (Eilers and Peeters 1988). Model parameters (α, β, and γ) were estimated by nonlinear regression with the Solver function in Microsoft Excel.

NPQ and ETR light-response curves were analyzed separately for each inhibitor using repeated-measures linear mixed-effects models. For each analysis, strain (HYU5231 and UTEX 2505) and treatment (control and inhibitor-treated) were included as between-subject fixed factors, whereas PAR was treated as a within-subject repeated factor because measurements were obtained sequentially from the same biological replicate across increasing PAR levels. All two-way and three-way interactions among strain, treatment, and PAR were included in the model. Biological replicate was included as a random effect to account for repeated measurements within the same culture. The strain × treatment interaction was used to test whether the effect of each inhibitor differed between the two strains, and the strain × treatment × PAR interaction was used to determine whether these strain-specific treatment responses varied across the 20 steps of PAR gradient (1, 11, 36, 56, 81, 111, 146, 186, 231, 281, 336, 396, 461, 531, 611, 701, 801, 926, 1,076, and 1,251 μmol photons m^{-2} s^{-1}).

Statistical analysis

All experiments were conducted using three independent cultures (n = 3 biological replicates). For each biological replicate, three technical measurements were obtained. These three technical measurements were averaged to generate one culture-level value. Thus, three culture-level values (n = 3 biological replicates) were used for statistical analyses. For cell-area analysis, 100 cells measured from each independent culture were treated as within-culture subsamples and averaged to obtain one culture-level mean. Statistical comparisons of cell area were performed using the three culture-level means per strain (n = 3 biological replicates). Biomass productivity, growth, and other single-response variables were analyzed using Student's *t*-test in SPSS version 27 (IBM Corp., Armonk, NY, USA).

RESULTS AND DISCUSSION

Isolation of a red-pigmented *Haematococcus*-like strain from a freshwater rock pool

A reddish-brown microbial mat was observed in a shallow rock pool near the Hantan River Basin, Korea. Microscopic examination of the environmental samples revealed spherical cells with a red pigment resembling stress-stage *Haematococcus* cells (Fig. 1). After multiple rounds of purification on antibiotic-containing TAP agar plates, a stable monoclonal culture was developed and designated HYU5231. Because morphological characters alone are insufficient for accurate species-level identification of *Haematococcus*, we performed molecular and phylogenetic analyses (Aiube et al. 2024, Lee et al. 2025).

Molecular identification and phylogenetic placement of HYU5231

To confirm taxonomic classification, we amplified and sequenced three molecular markers: 18S rRNA, ITS, and rbcL. The corresponding sequences were submitted to GenBank under accession Nos. PX688068, PX691028, and PZ530604.

The 1,701 bp 18S rRNA gene sequence obtained via PCR amplification was analyzed and compared with sequences in the NCBI database. The sequence exhibited 96–100% similarity with *H. lacustris*. Phylogenetic analysis indicated that the isolate was part of the *Haematococcus* clade, distinctly separate from related genera such as *Dunaliella* and *Chlorella* (Fig. 2A). Comparison of the ITS sequence showed that the isolate was distinct from *H. rubens* and aligned with the *H. lacustris* lineage (Fig. 2B).

PCR amplification of the rbcL gene yielded a 5 kb product, which was substantially larger than the typical 1.4–1.5 kb size of the rbcL gene. Sequence analysis revealed the presence of two introns (764 and 1,878 bp) in the coding region. Immunoblotting confirmed that these introns were accurately processed, resulting in the production of a translated protein identical to that of *H. lacustris* UTEX 2505 (Supplementary Fig. S1). Only exon sequences were used for phylogenetic reconstruction. The resulting phylogenetic tree placed the isolate within the same lineage as *H. lacustris* and *H. pluvialis*, distinctly separating it from the outgroup taxa *Chlamydomonas* and *Tetradesmus* (Fig. 2C). Therefore, the isolated strain was designated *H. lacustris* HYU5231.

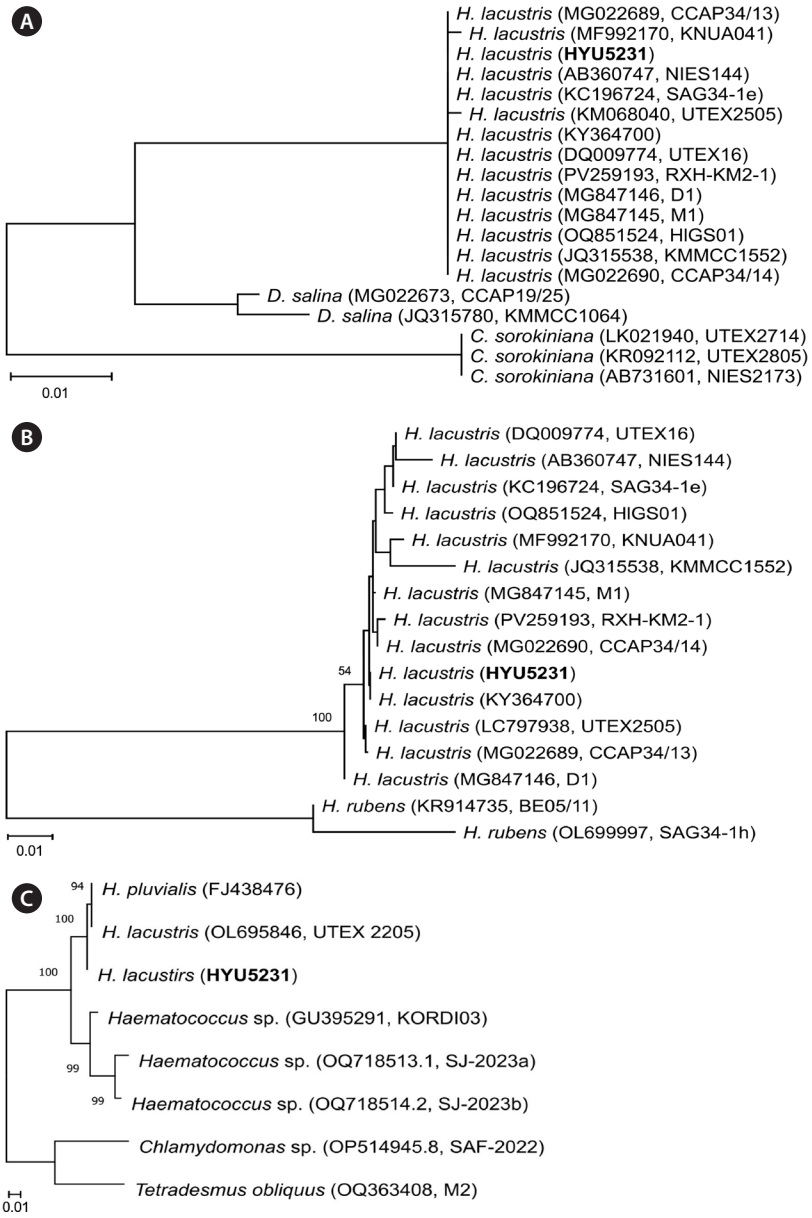


Fig. 2. Phylogenetic relationships inferred from 18S rRNA (A), internal transcribed spacer (ITS) (B), and rbcL gene sequences (C). Sequence alignment was carried out using MAFFT. Phylogenetic inference was performed in MEGA 11 using the neighbor-joining method for the 18S rRNA and ITS datasets and the maximum likelihood method for the rbcL dataset. Bootstrap analysis, with 500 replicates for 18S rRNA and 1,000 replicates for ITS and rbcL, was used to evaluate node support. The sequences downloaded and used for multiple sequence alignment and phylogenetic analyses are listed in Supplementary Table S1.

Morphological and physiological characteristics of HYU5231

After confirming the taxonomic identity of HYU5231 as *H. lacustris*, we investigated whether this newly isolated strain displayed unique physiological characteristics compared to the reference strain. Both *H. lacustris* strains HYU5231 and UTEX 2505 were cultivated under identical photoautotrophic conditions, and their morphology, pigmentation, growth, and biomass accumulation were compared.

Under the specified conditions, both strains remained in the green phase during cultivation, yet distinct differences were noted in the appearance of the culture and cellular morphology (Fig. 3A & B). HYU5231 cultures exhibited a paler green color than

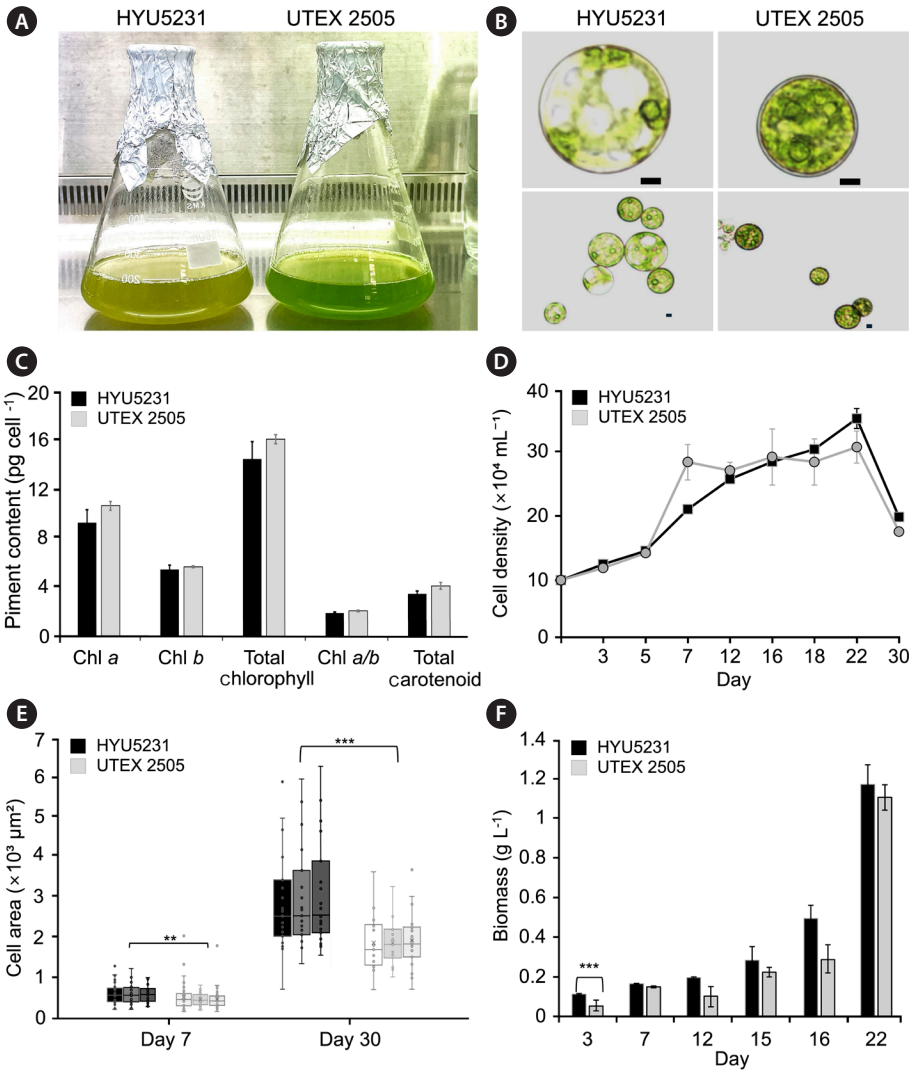


Fig. 3. Physiological characteristics of *Haematococcus lacustris* HYU5231 cultivated in Sueoka high salts (HS) medium. (A) Cultures of HYU5231 (left) and UTEX 2505 (right) grown in HS medium. HYU5231 has a lighter green color than UTEX 2505. (B) Stationary-phase cells of HYU5231 and UTEX 2505. HYU5231 cells contained less pigment than UTEX 2505 cells. Scale bars represent: upper, 20 μm; lower, 50 μm. (C) Comparison of pigment contents. (D) Growth curves derived from cell density. (E) Cell area distribution on days 7 and 30. The red-toned bars represent strain HYU5231, and the gray-toned bars represent UTEX 2505. Each of the three bars per strain represents the mean cell area of an independently cultivated biological replicate (n = 3). Differences between the two strains were evaluated using a two-tailed unpaired Student's *t*-test. **p < 0.01, ***p < 0.001. (F) Biomass accumulation of the two strains during cultivation. Data are presented as mean ± standard deviation from three independent cultures as biological replicates (n = 3). Statistical significance was evaluated using Student's *t*-test. ***p < 0.001.

UTEX 2505. Microscopic observations revealed that HYU5231 cells were significantly larger and contained prominent vacuole-like regions, whereas UTEX 2505 cells exhibited a more compact chloroplast structure.

Consistent with these morphological differences, HYU5231 contained lower levels of chlorophyll *a*, chlorophyll *b*, and carotenoids per cell than UTEX 2505 (Fig. 3C). Growth analysis indicated that both strains achieved similar cell densities during cultivation, although HYU5231 maintained slightly higher cell counts at later stages (Fig. 3D). Cell size analysis demonstrated that HYU5231 cells were significantly larger than UTEX 2505 cells on both days 7 and 30, with the size disparity becoming more evident with extended cultivation. Consistent with these observations, HYU5231 exhibited a larger cell area than UTEX 2505, with the maximum cell area being approximately 1.7 times greater (Supplementary Table S2). Statistical

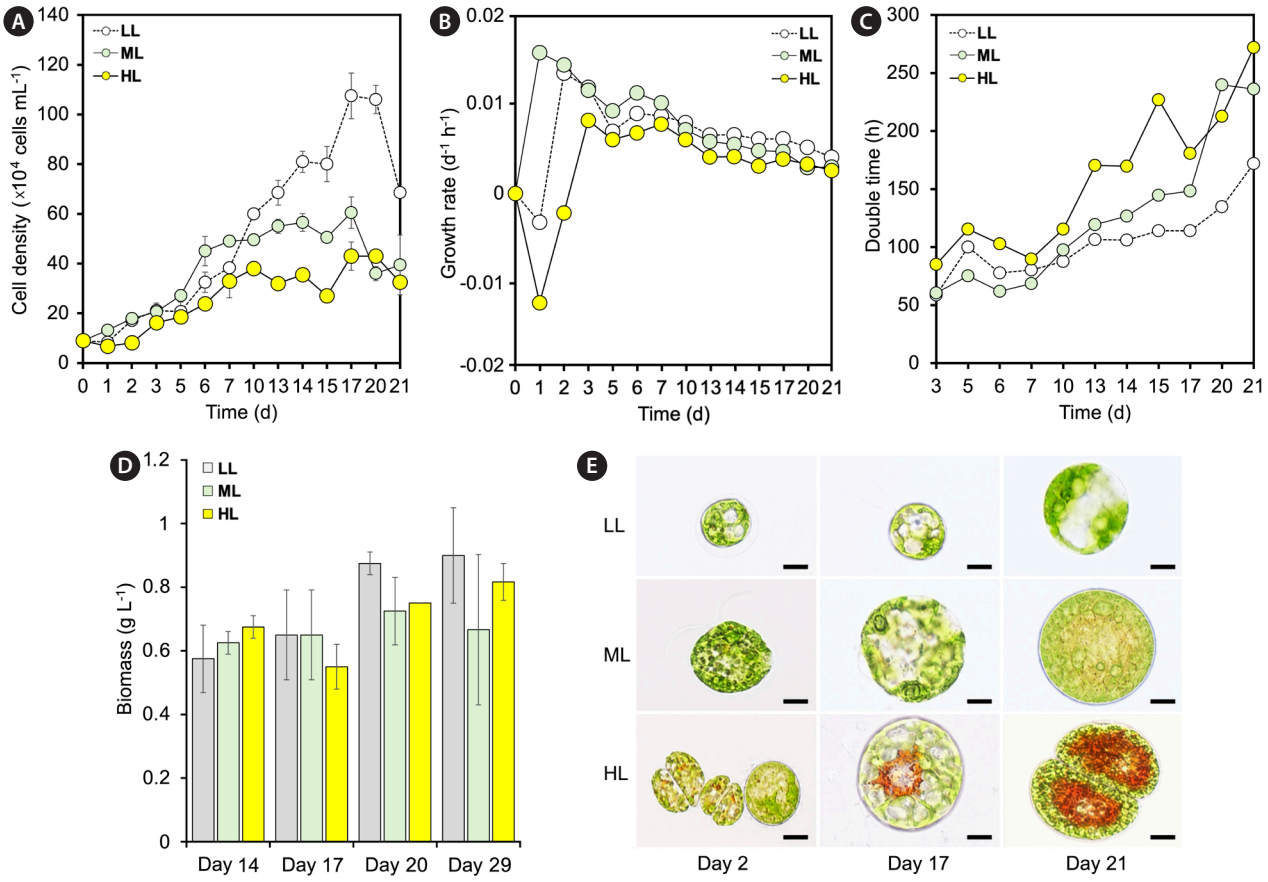


Fig. 4. Growth of *Haematococcus lacustris* HYU5231 under low-light (LL), medium-light (ML), and high-light (HL) conditions. (A) Cell density during cultivation. (B) Specific growth rate (μ) of HYU5231. (C) Doubling time during cultivation. (D) Biomass accumulation under varying light conditions. (E) Microscopy images of cells at different cultivation stages under LL, ML, and HL conditions. Data in (A–D) are shown as mean ± standard deviation from three independent biological replicates (n = 3). Scale bars represent: E, 10 μm.

analysis using Student's *t*-test confirmed that the difference in cell area was highly significant (***$p < 0.001$) (Fig. 3E). Despite these substantial differences in cell size and pigment content, biomass accumulation was comparable between the two strains throughout the cultivation period, with HYU5231 showing only a modest increase compared to UTEX 2505 at intermediate time points (Fig. 3F).

Overall, HYU5231 was distinguished by its larger cell size, lower pigment content per cell, and biomass productivity comparable to that of UTEX 2505, highlighting its distinct physiological traits despite its close phylogenetic relationships. Given that cell size is closely associated with cellular metabolism, resource allocation, and physiological performance in microalgae, the relatively larger cell size of HYU5231 further suggests potential metabolic differences compared with UTEX 2505 (Finkel et al. 2010).

Photoprotective responses of HYU5231 under increasing irradiance

When HYU5231 was cultivated under three different light intensities, an increase in irradiance led to a reduction in cell division (Fig. 4). Although growth was reduced at higher light intensities, the F_V/F_M was consistently above 0.5 across all light conditions during the cultivation period, indicating that PSII activity was largely maintained even under HL intensity conditions (Fig. 5A). In contrast, NPQ exhibited a strong light-dependent response. NPQ peaked on day 14 under all light conditions, with peak values of 0.44, 0.76, and 0.72 under LL (40 μmol photons m^{-2} s^{-1}), ML (150 μmol photons m^{-2} s^{-1}), and HL (500 μmol photons m^{-2} s^{-1}) intensities, respectively (Fig. 5B).

The pigment composition also changed markedly with irradiance. Under LL conditions, lutein, chloro-

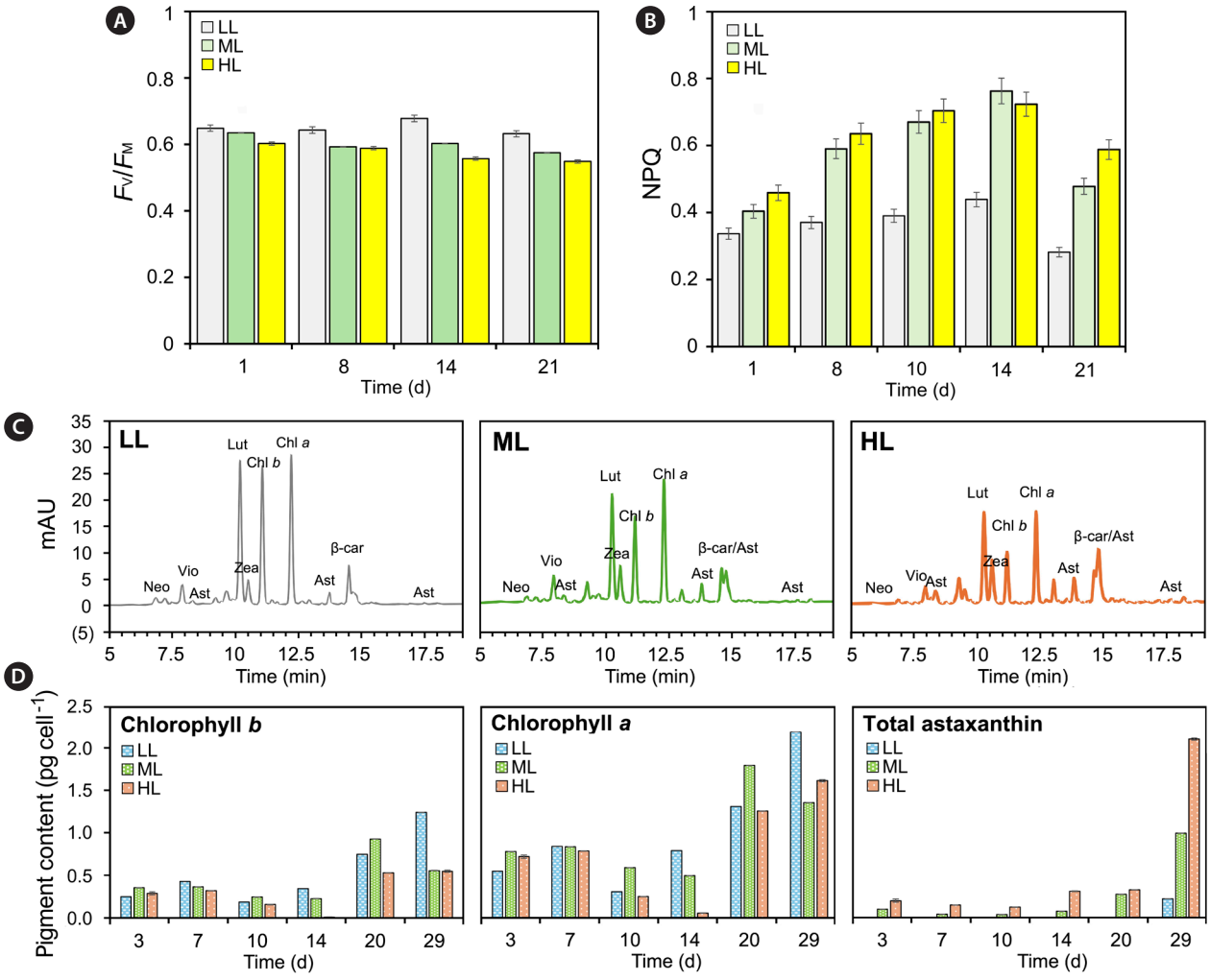


Fig. 5. Photosynthetic efficiency and pigment profile of HYU5231 under low-light (LL), medium-light (ML), and high-light (HL) conditions. (A) Maximum quantum yield of photosystem II (F_V/F_M) on days 1, 8, 14, and 21 of cultivation. (B) Non-photochemical quenching (NPQ) on days 1, 8, 10, 14, and 21 of cultivation. (C) High-performance liquid chromatography chromatograms of pigment extracts from cells grown under LL, ML, and HL conditions on day 14. Peaks indicate neoxanthin (Neo), violaxanthin (Vio), astaxanthin (Ast), zeaxanthin (Zea), lutein (Lut), chlorophyll *b* (Chl *b*), chlorophyll *a* (Chl *a*), and β-carotene (β-car). (D) Changes in chlorophyll *b*, chlorophyll *a*, and total astaxanthin contents on days 3, 7, 10, 14, 20, and 29 under different light conditions. Data in (A), (B), and (D) are shown as mean ± standard deviation from three independent biological replicates (n = 3).

phyll *a*, and chlorophyll *b* were relatively abundant, whereas ML and HL conditions resulted in reduced chlorophyll content and increased astaxanthin and carotenoid accumulation, with the effect being particularly pronounced under HL conditions (Fig. 5C & D, Supplementary Table S3). The reduction in chlorophyll content, accompanied by increased carotenoid accumulation under HL, likely represents an adaptive mechanism to limit excessive light absorption while enhancing photoprotection through carotenoid-mediated energy dissipation and reactive oxygen species (ROS) scavenging (Demmig-Adams 1990, Jahns and Holzwarth 2012). Increasing irradiance resulted in an increase in the DES of the xanthophyll pigments, with higher DES values observed under ML and HL conditions than under LL conditions on day 14 (Fig. 6A). The relative composition of violaxanthin, antheraxanthin, and zeaxanthin also changed over the cultivation period, with a greater proportion of de-epoxidized xanthophylls observed under ML and particularly HL conditions (Fig. 6B–D). These results indicate that HYU5231 adapts to elevated irradiance by expanding the pool of de-epoxidized xanthophylls, which may contribute to photoprotection under high-intensity light conditions.

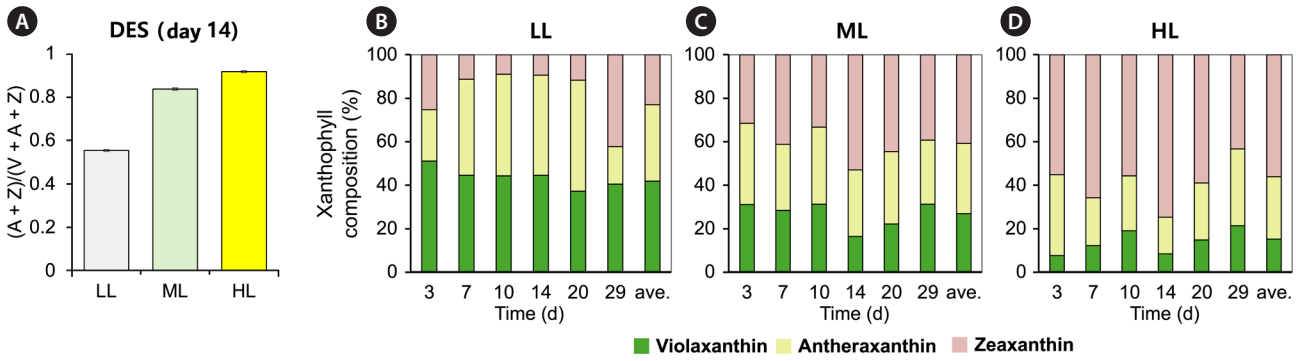


Fig. 6. Xanthophyll-cycle pigments in *Haematococcus lacustris* HYU5231 exposed to different light intensities. (A) De-epoxidation state (DES) on day 14 under low-light (LL), medium-light (ML), and high-light (HL) conditions. Values are shown as mean ± standard deviation from three independent biological replicates (n = 3). (B–D) Relative amounts of violaxanthin, antheraxanthin, and zeaxanthin over time under LL, ML, and HL conditions.

Notably, the rapid increase in astaxanthin content under HL conditions coincided with the peak of NPQ (Fig. 5D). This suggests that NPQ functions as the primary photoprotective mechanism during the initial stages of HL exposure, whereas astaxanthin accumulation becomes more important as light stress persists. Astaxanthin is known to protect photosynthetic cells by quenching singlet oxygen and other ROS, stabilizing cell membranes, and mitigating oxidative damage from high-intensity irradiance (Kobayashi et al. 1993, Boussiba 2000). Therefore, the coordinated induction of NPQ and astaxanthin biosynthesis in HYU5231 cells appears to constitute a complementary photoprotective strategy that enables the maintenance of PSII functionality under sustained high-light conditions.

These light-dependent responses suggest that HYU5231 activates a robust photoprotective response under excessive irradiance. However, the high NPQ observed in HYU5231 cannot be solely attributed to changes in pigment accumulation. Therefore, to further examine the mechanisms underlying this photoprotective phenotype, we analyzed NPQ and ETR after treatment with inhibitors targeting various components of photosynthetic electron transport.

Comparative inhibitor analysis of NPQ and relative electron transport in HYU5231 and UTEX 2505

To assess whether the high NPQ phenotype of HYU5231 was associated with xanthophyll cycle-dependent energy dissipation or alternative electron transport, HYU5231 and UTEX 2505 were treated with photosynthetic electron transport inhibitors and analyzed using PAM fluorometry.

Under control conditions, HYU5231 exhibited a rapid increase in NPQ, reaching values of approximately 0.8–1.0 at relatively low irradiance (100–200 µmol photons m^{-2} s^{-1}) and sustaining high NPQ throughout the tested light range. In contrast, the NPQ in UTEX 2505 increased gradually and reached a maximum value of approximately 0.4. The ETR of HYU5231 was approximately 10–15 µmol e^- m^{-2} s^{-1}, whereas UTEX 2505 exhibited higher ETR values of approximately 15–17 µmol e^- m^{-2} s^{-1}, indicating distinct strategies for light energy utilization and dissipation between the two strains. These findings collectively suggest that HYU5231 tends to dissipate excess excitation energy rather than sustaining high linear electron transport with increasing irradiance.

To further elucidate the mechanisms underlying the high NPQ phenotype of HYU5231, we examined the effects of inhibitors targeting distinct components of photosynthetic electron transport and photoprotection. DTT was used to assess the role of xanthophyll cycle-dependent NPQ, whereas PG and MV were used to assess the potential involvement of PTOX-associated electron flow and limitations on the photosystem I (PSI)-side electron acceptor, respectively.

DTT, which inhibits violaxanthin de-epoxidase and suppresses xanthophyll cycle-dependent NPQ, had minimal effect on NPQ or ETR in HYU5231 cells ($p = 0.386$). In contrast, DTT almost completely eliminated NPQ in UTEX 2505 cells and significantly increased ETR ($p < 0.001$). Repeated-measures linear mixed-effects analysis showed significant Strain × Treatment and Strain × Treatment × PAR interactions for both NPQ and ETR (Supplementary Tables S4 & S5), indi-

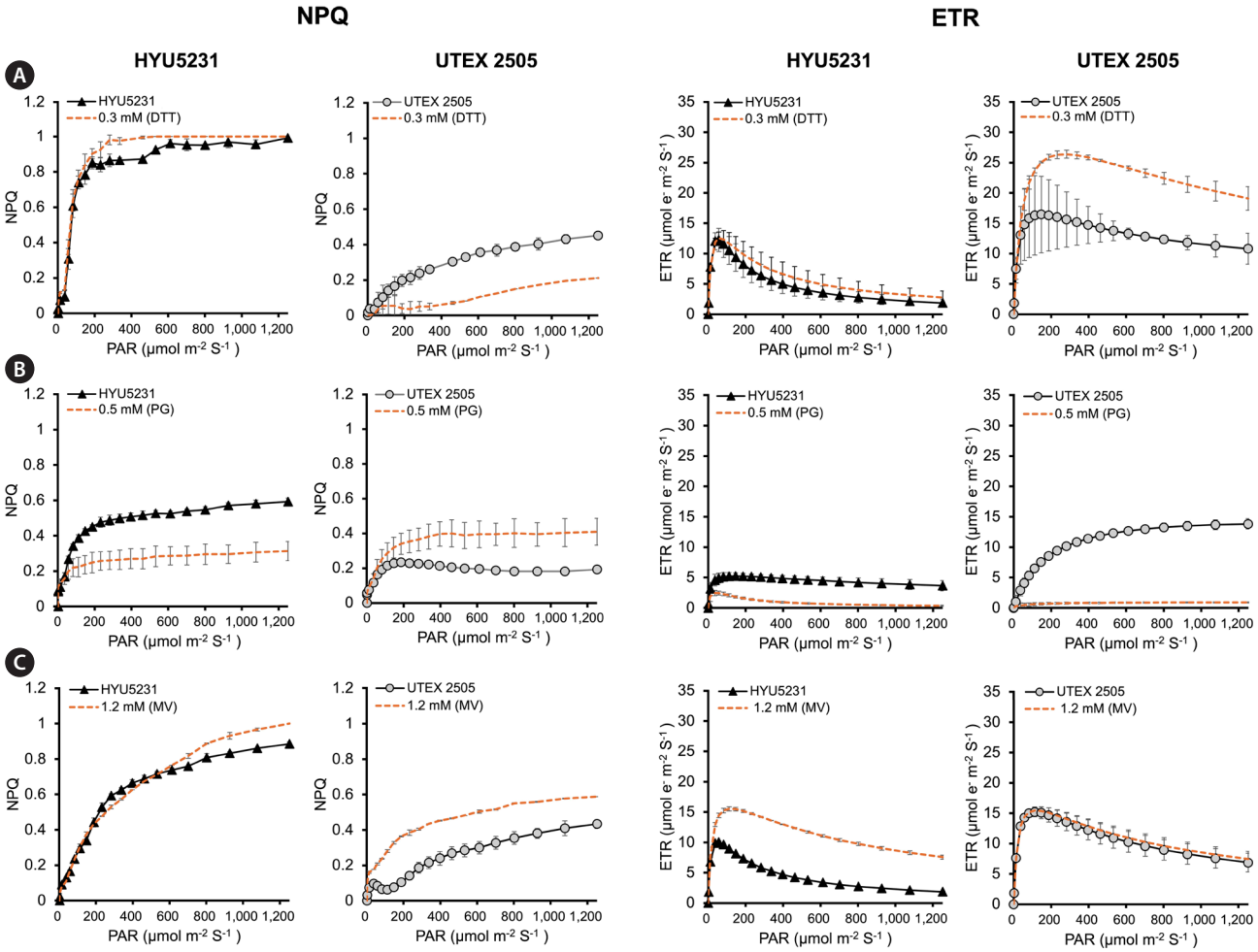


Fig. 7. Effects of photosynthetic inhibitors on non-photochemical quenching (NPQ) and electron transport rate (ETR) in *Haematococcus lacustris* HYU5231 and UTEX 2505. Panels (A), (B), and (C) show the effects of 0.3 mM dithiothreitol (DTT), an inhibitor of the xanthophyll cycle; 0.5 mM n-propyl gallate (PG), an inhibitor of plastid terminal oxidase; and 1.2 mM methyl viologen (MV), an artificial electron acceptor, respectively. For each treatment, NPQ (left two columns) and ETR (right two columns) were measured in HYU5231 and UTEX 2505 under increasing levels of photosynthetically active radiation (PAR) and compared with untreated controls. Data are presented as the mean ± standard deviation of three independent cultures as biological replicates (n = 3). Statistical analyses were performed as described in the Materials and Methods. Detailed results of the repeated-measures linear mixed-effects analyses and Tukey-adjusted pairwise comparisons are provided in Supplementary Tables S4 & S5.

cating that the effects of DTT differed between UTEX 2505 and HYU5231 and varied across the PAR gradient. Pairwise comparisons showed that DTT significantly increased NPQ only in HYU5231, whereas a significant change in ETR was detected only in UTEX 2505. These results suggest that NPQ formation in UTEX 2505 is primarily dependent on a DTT-sensitive pathway, whereas HYU5231 utilizes a different photoprotective mechanism to maintain NPQ (Fig. 7A). The reduction of NPQ by DTT treatment and its connection to the inhibition of the xanthophyll cycle have been reported in earlier studies (Bilger and Björkman 1990, Demmig-Adams 1990). Therefore, persistent NPQ in HYU5231 cells despite DTT treatment suggests the involvement of a xanthophyll cycle-independent photoprotective mechanism.

Conversely, treatment with the PTOX inhibitor PG produced the opposite effect. NPQ was markedly reduced in HYU5231 cells but increased in UTEX 2505 cells. ETR was only slightly affected in HYU5231 cells but was almost completely suppressed in UTEX 2505. Significant Strain × Treatment and Strain × Treatment × PAR interactions were detected for both NPQ and ETR under PG treatment (Supplementary Table S4). Pairwise comparisons showed that PG significantly increased NPQ in UTEX 2505 but decreased NPQ in

HYU5231. ETR decreased significantly in both strains, although the responses differed across PAR levels (Supplementary Table S5). Since the proton gradient across the thylakoid membrane (ΔpH) is a major factor driving NPQ induction and PTOX-associated alternative electron flow may contribute to ΔpH formation, the substantial reduction in NPQ following PG treatment may be associated with the inhibition of PTOX activity. This pronounced response in HYU5231, compared with UTEX 2505, is consistent with a possible contribution of PTOX-associated electron flow to NPQ induction in this strain (Fig. 7B).

Treatment with MV, a potent artificial electron acceptor, affected ETR differently between the two strains across the PAR gradient. In HYU5231, MV-treated cells showed higher ETR than untreated cells at higher irradiance, whereas little difference was observed in UTEX 2505 (Fig. 7C). Thus, the effect of MV on ETR was strain-specific and was most evident over the higher irradiance range. MV treatment also increased NPQ in both strains, although the magnitude and pattern of the response across the PAR gradient differed between strains, with a greater increase in UTEX 2505. Significant Strain × Treatment and Strain × Treatment × PAR interactions were detected for NPQ (Supplementary Table S4). Pairwise comparisons showed significant increases in NPQ in both strains (Supplementary Table S5). Because of the low ETR and NPQ values at low PAR levels, the strain-specific effects of DTT on NPQ and MV on ETR showed limited statistical significance under low irradiance. However, additional PAR-specific analyses confirmed that these strain-dependent differences became statistically significant as PAR increased (Supplementary Table S6). The strong enhancement of ETR in HYU5231 indicates that photosynthetic electron flow can be stimulated when the availability of PSI-side electron acceptors increases. This observation suggests that electron transport in HYU5231 cells may be constrained downstream of PSI, which was alleviated by MV treatment, as previously noted (Asada 1999).

A similar function for PTOX-dependent alternative electron flow has been observed in *Ostreococcus*, where PTOX acts as a photoprotective electron sink by oxidizing plastoquinol and preventing over-reduction of the photosynthetic electron transport chain under conditions of acceptor-side limitations (Cardol et al. 2008). In higher plants, PTOX works alongside the chloroplast NDH (NAD(P)H dehydrogenase) complex to maintain the redox balance of the PQ pool (Shikanai et al. 2025). However, in microalgae that lack the NDH complex, an alternative mechanism has been suggested, where Nda2 collaborates with PTOX as a "safety valve" thereby preventing PSI over-reduction (Houyoux et al. 2011). Consistent with this framework, the strong suppression of NPQ by PG and the increase in ETR by MV in HYU5231 cells suggest that PTOX may play a role in sustaining electron flow and photoprotection when electron acceptors downstream of PSI are limited. However, these results provide only indirect evidence. Further analyses, such as electrochromic shift measurements under control and PTOX-suppressed conditions and P700 oxidation kinetics, are necessary to validate this interpretation.

CONCLUSION

In this study, we identified and characterized HYU5231, a Korean variant of *H. lacustris*, demonstrating its unique photoprotective characteristics compared to the reference strain UTEX 2505. HYU5231 exhibited consistent PSII efficiency under increasing irradiance, while exhibiting strong NPQ induction and enhanced accumulation of astaxanthin and carotenoids. These findings suggest that rapid excitation energy dissipation and sustained antioxidant pigment accumulation shield HYU5231 cells from excess light.

Inhibitor studies revealed that NPQ in HYU5231 was largely unaffected by DTT but strongly suppressed by PG, whereas MV markedly increased relative electron transport. These observations suggest that HYU5231 has a xanthophyll cycle-independent photoprotective component, and that PTOX-related alternative electron transport may contribute to its high-NPQ phenotype under PSI acceptor-side limitations. To validate this mechanism, further investigations, including the direct assessment of PTOX activity, P700 redox kinetics, and electrochromic shift assessments, are necessary. Overall, HYU5231 is a distinct natural *Haematococcus* isolate with potential significance for studies on photoprotection, stress tolerance, and astaxanthin-related biotechnology.

ACKNOWLEDGEMENTS

This work was supported by Korea Environment Industry & Technology Institute (KEITI) through the Project for the Development of Technologies to Ensure Aquatic Ecosystem, funded by the Ministry of Envi-

ronment (MOE) of the Republic of Korea (RS-2025-02223263).

CONFLICTS OF INTEREST

The authors declare that they have no potential conflicts of interest.

DATA AND ALGAL STRAIN AVAILABILITY

The raw sequence data generated in this study have been deposited in the National Center for Biotechnology Information (NCBI) GenBank database under accession numbers PZ530604, PX688068, PX691028 for rbcL, 18S rDNA, and ITS respectively, and are listed in Supplementary Table S1.

The *Haematococcus lacustris* strain HYU5231 has been deposited in the Freshwater Bioresources Culture Collection (FBCC) under the accession number (FBCC-A1753), and will be available from the FBCC once it is released for public distribution.

SUPPLEMENTARY MATERIALS

Supplementary Table S1. Sequences used for multiple sequence alignment and phylogenetic analyses (https://www.e-algae.org).

Supplementary Table S2. ROI-based cell area measurements ($\times 10^3$ μm^2) (https://www.e-algae.org).

Supplementary Table S3. Pigment content per cell in HYU5231 cells cultured under low-light (LL), medium-light (ML), and high-light (HL) conditions during mid- and late-log phases of growth (https://www.e-algae.org).

Supplementary Table S4. Repeated-measures linear mixed-effects analysis of NPQ and ETR light-response curves following dithiothreitol (DTT, 0.3 mM), propyl gallate (PG, 0.5 mM), and methyl viologen (MV, 1.2 mM) treatments (https://www.e-algae.org).

Supplementary Table S5. Selected Tukey-adjusted pairwise comparisons of estimated marginal means for NPQ and ETR after dithiothreitol (DTT), propyl gallate (PG), and methyl viologen (MV) treatments (https://www.e-algae.org).

Supplementary Table S6. PAR-specific contrasts of strain-dependent responses of NPQ to dithiothreitol (DTT) and ETR to methyl viologen (MV) (https://www.e-algae.org).

Supplementary Fig. S1. SDS-PAGE and Western blot analyses (https://www.e-algae.org).

REFERENCES

Aiube, Y. R. A., Moreira, A. P. B., Villela, L. B., et al. 2024. Occurrence of the thermotolerant zoochlorellae *Symbiochlorum hainanense* associated with hydrocorals in the Southwestern Atlantic Ocean. Algae 39:241–253. doi.org/10.4490/algae.2024.39.11.11

Asada, K. 1999. The water-water cycle in chloroplasts: scavenging of active oxygens and dissipation of excess photons. Annu. Rev. Plant Biol. 50:601–639. doi.org/10.1146/annurev.arplant.50.1.601

Azúa-Bustos, A., González-Silva, C., Salas, L., Palma, R. E. & Vicuña, R. 2010. A novel subaerial *Dunaliella* species growing on cave spiderwebs in the Atacama Desert. Extremophiles 14: 443–452. doi.org/10.1007/s00792-010-0322-7

Bilger, W. & Björkman, O. 1990. Role of the xanthophyll cycle in photoprotection elucidated by measurements of light-induced absorbance changes, fluorescence and photosynthesis in leaves of *Hedera canariensis*. Photosynth. Res. 25:173–185. doi.org/10.1007/BF00033159

Boussiba, S. 2000. Carotenogenesis in the green alga *Haematococcus pluvialis*: cellular physiology and stress response. Physiol. Plant. 108:111–117. doi.org/10.1034/j.1399-3054.2000.108002111.x

Cardol, P., Bailleul, B., Rappaport, F., et al. 2008. An original adaptation of photosynthesis in the marine green alga *Ostreococcus*. Proc. Natl. Acad. Sci. U. S. A. 105:7881–7886. doi.org/10.1073/pnas.0802762105

Carol, P. & Kuntz, M. 2001. A plastid terminal oxidase comes to light: implications for carotenoid biosynthesis and chlororespiration. Trends Plant Sci. 6:31–36. doi.org/10.1016/S1360-1385(00)01811-2

Correa-Galvis, V., Redekop, P., Guan, K., et al. 2016. Photosystem II subunit PsbS is involved in the induction of LHCSR protein-dependent energy dissipation in *Chlamydomonas reinhardtii*. J. Biol. Chem. 291:17478–17487. doi.org/10.1074/jbc.M116.737312

Demmig-Adams, B. 1990. Carotenoids and photoprotection in plants: a role for the xanthophyll zeaxanthin. Biochim. Biophys. Acta Bioenerg. 1020:1–24. doi.org/10.1016/0005-2728(90)90088-L

Eilers, P. H. C. & Peeters, J. C. H. 1988. A model for the relationship between light intensity and the rate of photosynthesis in phytoplankton. Ecol. Modell. 42:199–215. doi.org/10.1016/0304-3800(88)90057-9

Fawley, M. W. & Fawley, K. P. 2004. A simple and rapid technique for the isolation of DNA from microalgae. J. Phycol. 40:223–225. doi.org/10.1111/j.0022-3646.2004.03-081.x

Finkel, Z. V., Beardall, J., Flynn, K. J., Quigg, A., Rees, T. A. V. & Raven, J. A. 2010. Phytoplankton in a changing world: cell size and elemental stoichiometry. J. Plankton Res. 32:119–137. doi.org/10.1093/plankt/fbp098

Houyoux, P.-A., Ghysels, B., Lecler, R. & Franck, F. 2011. In-

terplay between non-photochemical plastoquinone reduction and re-oxidation in pre-illuminated *Chlamydomonas reinhardtii*: a chlorophyll fluorescence study. Photosynth. Res. 110:13–24. doi.org/10.1007/s11120-011-9686-5

Imamoglu, E., Vardar Sukan, F. & Conk Dalay, M. 2007. Effect of different culture media and light intensities on growth of *Haematococcus pluvialis*. Int. J. Nat. Eng. Sci. 1:5–9.

Jahns, P. & Holzwarth, A. R. 2012. The role of the xanthophyll cycle and of lutein in photoprotection of photosystem II. Biochim. Biophys. Acta Bioenerg. 1817:182–193. doi.org/10.1016/j.bbabio.2011.04.012

Kim, M., Oh, H. J., Nguyen, K. & Jin, E. 2022. Identification and characterization of *Dunaliella salina* OH214 strain newly isolated from a saltpan in Korea. Algae 37:317–329. doi.org/10.4490/algae.2022.37.9.13

Kobayashi, M., Kakizono, T. & Nagai, S. 1993. Enhanced carotenoid biosynthesis by oxidative stress in acetate-induced cyst cells of a green unicellular alga, *Haematococcus pluvialis*. Appl. Environ. Microbiol. 59:867–873. doi.org/10.1128/aem.59.3.867-873.1993

Lacour, T., Babin, M. & Lavaud, J. 2020. Diversity in xanthophyll cycle pigments content and related nonphotochemical quenching (NPQ) among microalgae: implications for growth strategy and ecology. J. Phycol. 56:245–263. doi.org/10.1111/jpy.12944

Lee, H.-E., Kim, T., Kim, H.-S., Lee, O.-M. & Ki, J.-S. 2025. Evaluating nuclear (18S, ITS, and 28S) and chloroplast (*psbB*, *psbC*, *rbcL*, and *tufA*) genes of the green algae *Monoraphidium* (Sphaeropleales, Chlorophyta) for DNA barcoding. Algae 40:103–115. doi.org/10.4490/algae.2025.40.4.15

Maxwell, K. & Johnson, G. N. 2000. Chlorophyll fluorescence: a practical guide. J. Exp. Bot. 51:659–668. doi.org/10.1093/jexbot/51.345.659

Metting, F. B. Jr. 1996. Biodiversity and application of microalgae. J. Ind. Microbiol. Biotechnol. 17:477–489. doi.org/10.1007/BF01574779

Müller, P., Li, X.-P. & Niyogi, K. K. 2001. Non-photochemical quenching: a response to excess light energy. Plant Physiol. 125:1558–1566. doi.org/10.1104/pp.125.4.1558

Niyogi, K. K. & Truong, T. B. 2013. Evolution of flexible non-photochemical quenching mechanisms that regulate light harvesting in oxygenic photosynthesis. Curr. Opin. Plant Biol. 16:307–314. doi.org/10.1016/j.pbi.2013.03.011

Park, S., Jung, G., Hwang, Y.-S. & Jin, E. 2010. Dynamic response of the transcriptome of a psychrophilic diatom, *Chaetoceros neogracile*, to high irradiance. Planta 231:349–360. doi.org/10.1007/s00425-009-1044-x

Peers, G., Truong, T. B., Ostendorf, E., et al. 2009. An ancient light-harvesting protein is critical for the regulation of algal photosynthesis. Nature 462:518–521. doi.org/10.1038/nature08587

Ruban, A. V. 2016. Nonphotochemical chlorophyll fluorescence quenching: mechanism and effectiveness in protecting plants from photodamage. Plant Physiol. 170:1903–1916. doi.org/10.1104/pp.15.01935

Seckbach, J., Chapman, D. J., Garbary, D., Oren, A. & Reisser, W. 2007. Algae and cyanobacteria under environmental extremes: final comments. *In* Seckbach, J. (Ed.) *Algae and Cyanobacteria in Extreme Environments*. *Cellular Origin, Life in Extreme Habitats and Astrobiology. Vol 11.* Springer, Dordrecht, pp. 781–786. doi.org/10.1007/978-1-4020-6112-7_42

Shikanai, T., Ieda, H., Kobayashi, Y. & Tamura, M. N. 2025. The chloroplast NADH dehydrogenase-like complex: evolutionary considerations. Plant Cell Physiol. 66:1525–1535. doi.org/10.1093/pcp/pcaf046

Sueoka, N. 1960. Mitotic replication of deoxyribonucleic acid in *Chlamydomonas reinhardi*. Proc. Natl. Acad. Sci. U. S. A. 46: 83–91. doi.org/10.1073/pnas.46.1.83

Sun, H., Kong, Q., Geng, Z., Duan, L., Yang, M. & Guan, B. 2015. Enhancement of cell biomass and cell activity of astaxanthin-rich *Haematococcus pluvialis*. Bioresour. Technol. 186:67–73. doi.org/10.1016/j.biortech.2015.02.101

Teoh, M.-L., Phang, S.-M. & Chu, W.-L. 2013. Response of Antarctic, temperate, and tropical microalgae to temperature stress. J. Appl. Phycol. 25:285–297. doi.org/10.1007/s10811-012-9863-8

Won, H., Ro, E., Seo, S., Kim, B. H. & Jin, E. 2023. Isolation and cultivation of freshwater diatom *Nitzschia palea* HY1 for increasing biomass and fucoxanthin production. Algae 38:191–202. doi.org/10.4490/algae.2023.38.9.3

Yuan, J.-P. & Chen, F. 2000. Purification of trans-astaxanthin from a high-yielding astaxanthin ester-producing strain of the microalga *Haematococcus pluvialis*. Food Chem. 68:443–448. doi.org/10.1016/S0308-8146(99)00219-8